Spin-reorientation transition and magnetic phase diagrams of thin epitaxial Au(111)/Co films with W and Au overlayers

R. Sellmann, H. Fritzsche, and H. Maletta*

Hahn-Meitner-Institut Berlin, Glienicker Strasse 100, D-14109 Berlin, Germany

V. Leiner and R. Siebrecht

Institut Laue Langevin, BP 156, F-38042 Grenoble Cedex 9, France

We present a study of the thickness- and temperature-driven spin-reorientation transition in thin epitaxial Au(111)/Co films grown on single-crystal sapphire $Al_2O_3(11\bar{2}0)$ substrates. The transition as a function of Co film thickness was investigated *in situ* at $T=300$ K by means of the magneto-optical Kerr effect at Co wedge-shaped samples prior and after coverage with W and Au overlayers. The thermal-induced transition, in particular the evolution and stability of in-plane and out-of-plane magnetization components, was studied in the temperature range from 10 to 300 K by reflectivity experiments with polarized neutrons and angular-dependent measurements with superconducting quantum interference device magnetometry. Magnetic phase diagrams, as determined by extended measurements on Au(111)/Co/Au and Au(111)/Co/W show that for the former films the perpendicular anisotropy is stable over a larger thickness region at low temperature.

I. INTRODUCTION

Magnetic anisotropy describes the dependence of the free energy on the magnetization direction in a magnetic system and is therefore of great importance for the magnetism of condensed matter and its technical applications. The main sources of magnetic anisotropy are the magnetic dipole-dipole interaction and the spin-orbit interaction, which lead to certain forms of appearance, essentially the shape anisotropy and magnetocrystalline anisotropy. While the first is strongly dependent on the shape of the sample, the second reflects the symmetry of the underlaying crystal lattice. Néel[1] pointed out that for atoms near the surface additional contributions to the magnetic anisotropy arise, due to their modified surrounding. In this sense, one distinguishes between volume and surface anisotropy contributions. In thin films, the ratio of surface or interface atoms to the total amount of the film atoms is relatively large and therefore the surface contribution is no longer negligible. As a rule, the volume contribution is governed by the shape anisotropy, which always favors a magnetization direction parallel to the film plane. In contrast to this, the surface contribution may favor either an in-plane or an out-of-plane direction of magnetization. By changing the film thickness in the latter case, one may induce a spin-reorientation transition (SRT), i.e., a change of the easy axis of magnetization, at values of film thickness, at which the anisotropy contributions are in balance with each other. Since magnetic anisotropies are generally temperature dependent, a SRT may also be induced thermally.

If we restrict ourselves to a discussion of polar anisotropies, i.e., if we consider only the polar angle θ between the magnetization and film normal and neglect dependences on the azimutal angle ϕ, then the free anisotropy energy $f(\theta)$ per volume of a thin magnetic film may be expressed by the following power series:[2,3]

$$f(\theta)=f_0+K_2 \sin^2 \theta + K_4 \sin^4 \theta + \cdots, \quad (1)$$

with the thickness- and temperature-dependent anisotropy coefficients of second (K_2) and fourth (K_4) order. The most common ansatz for the separation of volume and surface contributions is given by[4–6]

$$K_i(d,T)=K_i^V(T)+\frac{2K_i^S(T)}{d}, \quad i=2,4 \quad (2)$$

with the film thickness d, the temperature T, and the volume and surface anisotropy coefficients K_i^V and K_i^S of ith order. These are essentially coefficients of the magnetocrystalline anisotropy, with the exception of K_2^V, which also contains the shape anisotropy coefficient $-\frac{1}{2}\mu_0 M_S^2$, where M_S is the saturation value of the magnetization. For simplicity, we have assumed that the magnetic layer is bound by two identical interfaces, which explains the prefactor 2. Equation (2) is somewhat simplified, since lattice distortions and structural changes can lead to dependences of K_i^V and K_i^S on d, too.

Minimization of Eq. (1) gives three solutions for the equilibrium angle θ_{eq} of the magnetization: $\theta_{eq}=0$, $\theta_{eq}=\pi/2$, and $\theta_{eq}=\arcsin([-K_2/2K_4]^{0.5})$. For the transition from $\theta_{eq}=0$ (perpendicular magnetization) to $\theta_{eq}=\pi/2$ (in-plane magnetization) and vice versa, one can distinguish between three types[6]: (i) Continuous SRT ($K_4>0$): θ_{eq} changes continuously in the transition region with $\theta_{eq}=\arcsin([-K_2/2K_4]^{0.5})$. (ii) Discontinuous SRT ($K_4<0$): this transition is unsteady and, due to the existence of metastable states, irreversible. (iii) Special SRT($K_4\equiv0$): this transiton is unsteady but, in contrast to case (ii), reversible.

Within the framework of "anisotropy flow,"[7] one can describe a thickness-driven SRT by plotting the trajectory $\{K_2(d,T),K_4(d,T)\}_{T=const}$ in a K_2-K_4 diagram with the boundaries of the stable and metastable phases of θ_{eq}. In

general, these trajectories are not identical for different values of T. Thus, for certain values of d, trajectories $\{\cdots\}_{d=\text{const}}$ may also traverse a region of transition and describe a temperature-driven SRT. Obviously, the thickness- and temperature-driven SRT are closely related. However, from a theoretical point of view, the temperature-driven SRT is much more difficult to treat, since T is an implicit variable of K_2 and K_4 [see Eq. (2)] and both depend on it in a complicated way. Very often, one confines oneself to semiclassical spin models and performs calculations[8–10] within the framework of mean-field theory or Monte Carlo simulations[11–12] by use of Heisenberg-type models. Recently, the temperature-driven SRT has been investigated within an itinerant-electron model for the first time.[13]

Usually, the perpendicular anisotropy appears at small values of film thickness and at low temperature, as it was observed among others for the systems Cu(001)/Fe,[14,15] Ag(001)/Fe,[14,16] Cr(110)/Fe,[6,17] Ru(0001)/Co,[18] CeH$_2$/Co,[19] Pd(111)/Co,[20] and Au(111)/Co.[21–25] In contrast to this, the system Cu(001)/Ni exhibits an anomalous transition in a certain Ni thickness and temperature regime, i.e., a change of the easy axis of magnetization from the in-plane to the out-of-plane orientation with *increasing* Ni thickness and temperature, which can be explained by a magnetoelastic contribution to the magnetic anisotropy.[26,27] In some systems a SRT occurs within the film plane—for example, in W(110)/Fe (Refs. 28 and 29) and Au(111)/Fe (Ref. 30).

According to the Mermin-Wagner theorem,[31] a two-dimensional spin system with an isotropic, short-range interaction cannot exhibit any long-range magnetic order at finite temperatures. In addition to this, some theoretical studies of the temperature-driven SRT predict a loss of magnetic order at the transition.[32–34] A clear experimental proof has not been given yet. Bander and Mills showed for a two-dimensional Heisenberg system that arbitrarily small anisotropies are sufficient to stabilize long-range magnetic order.[35]

Experimental investigations of micromagnetic structures show that films with perpendicular anisotropy often decay in small domains[15] magnetized up and down. The domain configuration is frequently irregular, but in some cases the formation of a stripe pattern has also been observed. In theoretical work it was also shown that under certain conditions a domain structure in films with perpendicular anisotropy may be energetically more favorable than a single-domain state.[36–39] Domain structures are increasingly simulated by means of computers. Monte Carlo simulations yield configurations which are similar to configurations observed experimentally.[40,41]

In this paper, we present investigations of the thickness- and temperature-driven SRT in thin epitaxial Au(111)/Co films prepared on sapphire Al$_2$O$_3$(11$\bar{2}$0) single crystals, taking into account the effect of different Co/nonmagnetic metal interfaces as well. At room temperature, ultrathin uncovered Co(0001) layers prepared on Au(111) substrates exhibit a perpendicular magnetic anisotropy[22,24,25] in contrast to Co(0001) films grown on W(110) substrates.[42–44] Here we compare the thickness- and temperature-dependent anisotropy properties if W and Au are used as overlayer materials. Section II gives a description of the preparation and growth

of the samples. In Sec. III we present experiments dedicated to study the evolution of perpendicular magnetic anisotropy and details of the SRT as a function of Co thickness and temperature. These have been performed *in situ* by the magneto-optical Kerr effect (MOKE) and *ex situ* by polarized neutron reflectometry (PNR) and superconducting quantum interference device (SQUID) magnetometry. A summary of the main results is given in Sec. IV.

II. SAMPLE PREPARATION

The samples were prepared by molecular beam epitaxy in an ultrahigh-vacuum system[45] (base pressure $<3 \times 10^{-10}$ mbar). As substrates, we used one-side polished sapphire Al$_2$O$_3$(11$\bar{2}$0) single crystals. In PNR studies it is advantageous for reasons of intensity to choose substrates with a relative large area, while a commercial SQUID magnetometer requires sample sizes which amount to only a few square millimeters. Hence, in PNR and MOKE investigations, we used substrates with a areas of 30×15 and 39×15 mm^2, respectively, while we chose an area of 4×5 mm^2 for SQUID magnetometry. A relative large distance of 0.60 m between the evaporator and facing substrate ensures a homogeneous film thickness across the substrate area.

Prior to film deposition, the sapphire crystals were sputtered and annealed until they had a contaminant-free surface with a well-defined crystal order. The surface layer was well crystallized, as checked by Auger electron spectroscopy (AES) and low-energy electron diffraction (LEED). In order to grow an epitaxial Au(111) substrate layer, we first deposited an epitaxial W(110) buffer layer at a substrate temperature $T_p \approx 1200$ K. A deposition rate of $r_W = 0.05$ Å/s and a film thickness of $d_W \approx 100$ Å were chosen. After deposition, the substrate heater was turned off and the sample was allowed to cool down to room temperature at a natural rate. The LEED spots of the buffer layer were quite sharp, and their positions indicated the presence of a bcc (110) crystal structure. Onto the W(110) layer we deposited Au at $T_p = 300$ K with a rate $r_{Au} = 0.04$ Å/s and a thickness $d_{Au} = 30$ Å. LEED investigations of our Au film revealed the known fcc(111) diffraction pattern. The spots were somewhat broader in comparison to the LEED pattern of the W(110) buffer layer, but were still well defined.

For a growth study of Co on the Au(111) substrate layer, we prepared a wedge-shaped Co layer with an inclination of 0.79 Å/mm by translating the sample behind a mask during growth with a motor-controlled manipulator. The deposition was done at $T_p = 300$ K with a rate $n_{Co} = 0.036$ Å/s. At a film thickness of about two monolayers (2 ML) (1 ML$\cong$2 Å), one can recognize a LEED pattern with sixfold symmetry. With increasing Co film thickness, the spots sharpen. Further, an analysis of the relative distances of the LEED spots shows that the strained Co lattice is relaxing above a thickness of 2–3 ML. The relatively fast onset of relaxation has also been observed in previous studies[22,46,47] on Co/Au(111) and is attributed to the large in-plane lattice mismatch of about 14% between Au(111) and Co(0001), which is relieved by emerging misfit dislocations.[2,46]
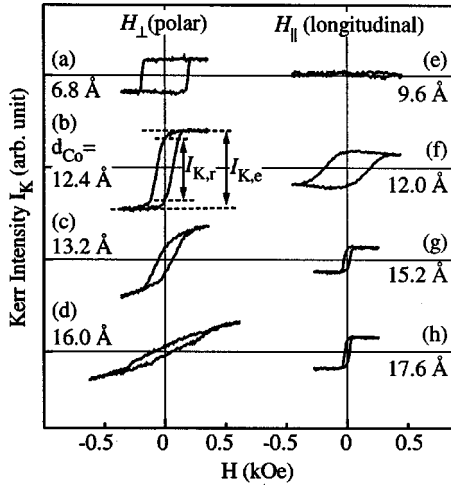
The Co layers of our samples were covered either with W

FIG. 1. Hysteresis loops of a wedge-shaped sample Au(111)/d_{Co}Co/W measured at $T = 300$ K for magnetic fields applied perpendicular (left panel) and parallel (right panel) to the film plane. $I_{K,r}$ and $I_{K,e}$ denote the remanent and extrapolated Kerr signals (see text).

or Au at $T_p = 300$ K. In both cases the overlayer thickness was 30 Å, which is sufficient to cover the Co layer completely (the Auger electron spectra were free of Co peaks), without reducing considerably the signal-to-noise ratio in MOKE measurements. Samples for *ex situ* experiments were prepared with about 200-Å-thick Au overlayers. Such additional, thick overlayers are advantageous in PNR measurements, since they shift the Kiessig fringes, which correspond to the total thickness of the layered system, to smaller values of the scattering vector. Differences in the reflectivity between spin-up and spin-down neutrons are measured more sensitively in this way.[48]

III. SPIN-REORIENTATION TRANSITION AND MAGNETIC PHASE DIAGRAMS

A. Thickness-driven SRT

We studied *in situ* the thickness-driven SRT in epitaxial Co wedge-shaped layers on Au(111) at $T = 300$ K by MOKE prior and after deposition of W and Au overlayers. The light source was a He-Ne laser ($\lambda = 632.8$ nm). The basic detection scheme consisted of a lock-in amplifier combined with a photoelastic modulator, which was placed between two polarizers. The amplitude of the laser beam was modulated with a frequency of 100.24 kHz.

Figure 1 shows some Kerr loops measured on a cobalt wedge-shaped sample on Au(111) after coverage with W. The inclination of the wedge was 0.79 Å/mm, while the diameter of the laser spot on the sample was about 0.3 mm, which results in a spatial resolution of the Co film thickness of about 0.2 Å. We denote measurements in the longitudinal geometry as $H_\parallel$ (**H** parallel to the film plane) and measurements in the polar geometry as $H_\perp$ (**H** perpendicular to the film plane). As shown in Fig. 1, the *remanent Kerr signal* $I_{K,r}$ is given by the difference of the intensity between both

TABLE I. Characteristic Co thicknesses $d_{Co,c\perp}$, d_{Co}^*, and $d_{Co,c\parallel}$ of the thickness-driven SRT at $T = 300$ K for Au(111)/Co without (UHV) and with W and Au overlayers determined with MOKE. For $d_{Co} < d_{Co,c\perp}$ ($d_{Co} > d_{Co,c\parallel}$), the perpendicular (in-plane) magnetization is stable. d_{Co}^* is the Co thickness at which the polar Kerr suscepibility in the remanent state is maximum.

	$d_{Co,c\perp}$	d_{Co}^*	$d_{Co,c\parallel}$
Au(111)/Co/UHV	8.8	9.6	10.0
Au(111)/Co/W	11.7	12.8	14.8
Au(111)/Co/Au	12.6	14.5	20.1

branches of the loop at $H = 0$. The *extrapolated Kerr signal* $I_{K,e}$ is obtained by extrapolation of the Kerr data at each end of the loop to $H = 0$.

In our measurements we find three regions of film thickness d_{Co} separated by the characteristic thicknesses $d_{Co,c\perp}$ and $d_{Co,c\parallel}$, with values of $d_{Co,c\perp}$ and $d_{Co,c\parallel}$ summarized in Table I. In region I ($d_{Co} < d_{Co,c\perp}$), $I_{K,e}$ increases with d_{Co} for $H_\perp$. The hysteresis loops have a rectangular shape with $I_{K,r} \approx I_{K,e}$ [Fig. 1(a)]. For $H_\parallel$ we find $I_{K,r} \approx 0$ and $I_{K,e} \approx 0$ [Fig. 1(e)]. In region I the shape anisotropy is overcompensated by the interface anisotropy, which leads to a perpendicular anisotropy. In region II ($d_{Co,c\perp} \lesssim d_{Co} \lesssim d_{Co,c\parallel}$), $I_{K,r}$ starts to decrease for $H_\perp$ with respect to $I_{K,e}$. The hysteresis loops are losing their rectangular shape. Both branches take on an S-like curve [Figs. 1(b) and 1(c)]. The reduction of remanence indicates that the perpendicular orientation of magnetization is becoming unstable. If d_{Co} is further increased by a small amount, $I_{K,r}$ continues decreasing, and now $I_{K,e}$ starts to decrease, too [compare Fig. 1(b) with Fig. 1(c)]. For the moment, we only mention that in this region one possibly observes in-plane hysteresis loops with relative large values of $I_{K,r}$ and $I_{K,e}$ and coercive fields H_c [Fig. 1(f)]. This will be discussed below. In region III ($d_{Co} > d_{Co,c\parallel}$), we find hysteresis loops for $H_\parallel$ with small saturation and coercive fields and $I_{K,r} \approx I_{K,e}$ [Figs. 1(g) and 1(h)]. Now $I_{K,e}$ is increasing for $H_\parallel$ approximately linearly with d_{Co}. Here $I_{K,e}$ is smaller than for $H_\perp$ in region I, since a longitudinal Kerr signal is generally weaker than the corresponding polar Kerr signal.[49] The observed magnetization curves for $H_\perp$ are apart from small hysteresis effects characteristic for a hard axis [Fig. 1(c)]. In region III the magnetization is no longer stable in the out-of-plane orientation. Therefore, a thickness-driven SRT has taken place in region II. In the transition region, the polar hysteresis loops show a striking change of the Kerr signal near $H = 0$. This change may be expressed by the Kerr susceptibility $\chi_{K,r} = dI_K/dH|_{H=0}$ of the remanent state. Figure 2 shows the polar Kerr susceptibility $\chi_{K,r}$ for Au(111)/Co/W [and Au(111)/Co/Au] as a function of d_{Co}. In region I, $\chi_{K,r} \approx 0$, which is a consequence of the rectangular shape of the hysteresis loops. In region II, $\chi_{K,r}$ strongly increases in a narrow thickness interval and reaches a maximum at $d_{Co} = d_{Co}^*$. This jumplike increase marks a pronounced reduction of $I_{K,r}$ with respect to $I_{K,e}$ and indicates that the single-domain state of perpendicular magnetization in region I, which is character-
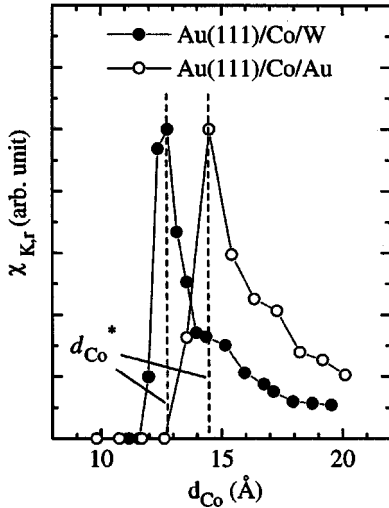
FIG. 2. Polar Kerr susceptibility $\chi_{K,r}$ in the remanent state at $T = 300$ K of Au(111)/Co/W and Au(111)/Co/Au vs d_{Co}.
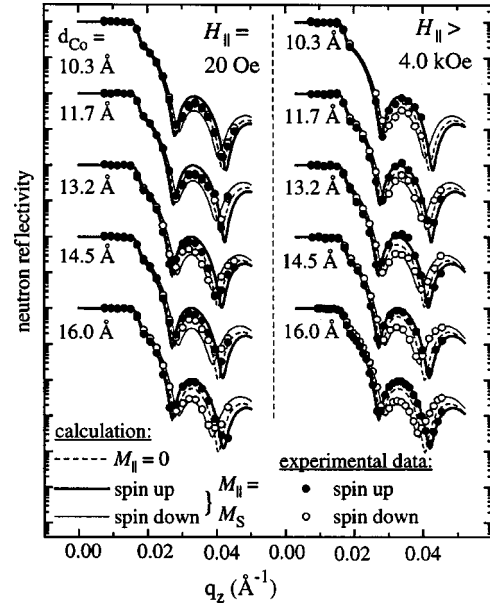

FIG. 3. Polarized neutron reflectivities of Au(111)/Co/W samples with different Co thickness d_{Co} measured for the approximately remanent (left panel) and the in-plane saturated (right panel) states at $T = 300$ K. The lines represent calculations for the in-plane (solid line) and out-of-plane (dashed line) saturated states.

ized by rectangular hysteresis loops, becomes unstable and possibly decays into domains near $H = 0$. The decrease of $\chi_{K,r}$ above d_{Co}^* accounts for the fact that the film normal becomes more and more a hard axis with increasing d_{Co}. The measured values of d_{Co}^* are listed in Table I.

The transition regions, which we found for our Au(111)/Co systems grown on $Al_2O_3(11\bar{2}0)$ substrates (Table I), are in good agreement with other studies of Au(111)/Co/UHV (Refs. 22 and 24) and Au(111)/Co/Au (Ref. 23). To our knowledge, the system Au(111)/Co/W has not been studied up to now, only the system W(110)/Co/Au.[43] Our results show that the coverage with W leads to a shift of the SRT region to larger values of the Co film thickness, which is somewhat smaller than for a Au coverage at $T = 300$ K.

As already mentioned, in-plane hysteresis loops with unusual large Kerr signals and coercive fields [Fig. 1(f)] may appear in the transition region. We assume that, as for the system Ag(100)/Fe,[16] this appearance is caused by the dominant polar Kerr effect of out-of-plane magnetization components. In order to study the behavior of the in-plane magnetization in the transition region in more detail, we performed measurements with PNR. The particular value of this method[48,50–53] is that it allows one to determine the absolute magnetic moments of the individual layers in a stack. In our experiment, we profit from the fact that the neutrons are only sensitive to the in-plane magnetization and no superimposing contribution from perpendicular magnetization has to be taken into account. We prepared five samples of the type $Al_2O_3(11\bar{2}0)/W(110)/Au(111)/Co/W/Au$ with different d_{Co} (no wedges). In Fig. 3 spin-dependent reflectivities measured at the neutron reflectometer V6 (HMI, Berlin) (Ref. 54) at $T = 300$ K are shown for the remanent (left panel) and magnetic (right panel) saturated state. The neutrons are polarized either parallel (spin up) or antiparallel (spin down) with respect to the external magnetic field **H**, which is applied parallel to the film plane and perpendicular to the incoming neutron beam. To prevent a depolarization of the neutrons

outside the sample, a small guide field of 20 Oe is always present. As usual, q_z denotes the z component of the scattering vector $\mathbf{q} = \mathbf{k}_f - \mathbf{k}_i$, where $\mathbf{k}_i$ and $\mathbf{k}_f$ are the wave vectors of the incoming and reflected neutron waves. The lines represent model calculations,[55] which are based on the Parratt formalism.[56] The *nuclear* scattering length densities of the individual layers and substrate are based on the values of Ref. 58. For the calculations of the *magnetic* scattering length density of the in-plane saturated state (solid lines), the spontaneous magnetization M_S of bulk hcp Co (Ref. 57) was assumed. Figure 3 shows that the experimental data for the in-plane saturated state agree well with the calculated reflectivities.

If the magnetization is aligned parallel to the film normal, one expects a vanishing splitting (dashed line) between the spin-up and spin-down reflectivities, since exclusively the in-plane component of the magnetization contributes to a spin-dependent reflection of neutrons.[59,60] The samples with $d_{Co} = 10.3$ and 11.7 Å do not show a significant spin dependence of the reflectivity in a weak magnetic field after saturation. As we have seen in the MOKE experiment, there is in fact a perpendicular magnetic anisotropy for these film thicknesses. The samples with $d_{Co} = 13.2$ and 14.5 Å are in the region of transition. Here a finite, but considerably reduced remanent in-plane magnetization is present. We can therefore conclude that the global magnetization is *tilted* with respect to the film plane. Further, we can now exclude an enhancement of the in-plane component in the transition region, as was pretended by the MOKE experiment. Finally, the spin dependence of the reflectivity pattern of the sample with $d_{Co} = 16.0$ Å at low field is only slightly reduced with respect to the saturated state. The easy axis of magnetization is now oriented in the film plane.
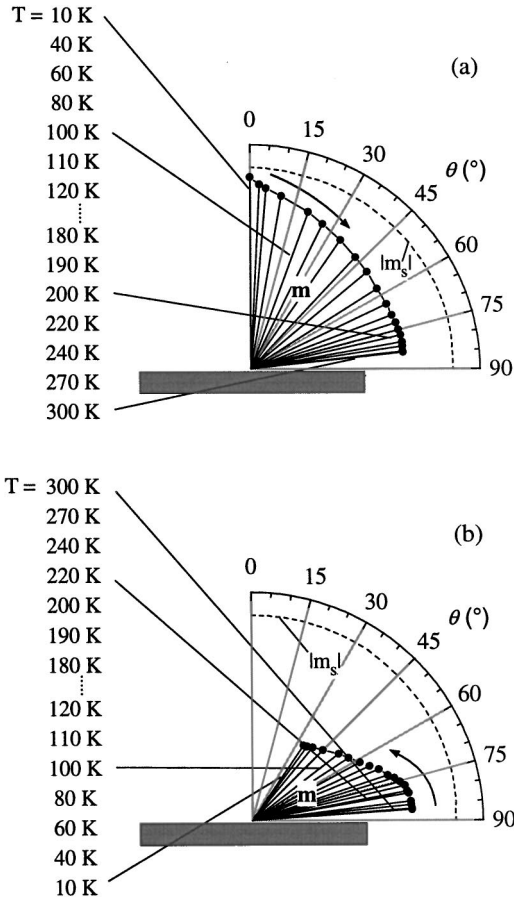
FIG. 4. Vector diagrams of the effective magnetic moment $\mathbf{m}(T)$ of a Au(111)/16.7 Å Co/W sample for (a) increasing and (b) decreasing temperature T.

B. Temperature-driven SRT

An interesting question is which way the perpendicular magnetization evolves with changing temperature. In this section, we present SQUID and PNR experiments which were dedicated to this aspect.

Figure 4 shows SQUID data measured for a Au(111)/Co/W sample with $d_{Co} = 16.7$ Å. We used a sample holder, which permitted us to rotate the sample in an axis perpendicular to the external magnetic field by means of a computer-controlled precision mechanism. The maximum absolute error of the angle θ_H between the external field and film normal amounts to about 3°. We corrected the data for the background signals of the sample holder and substrate. The dotted lines in Fig. 4 represent the bulk value of the magnetic saturation moment m_S for hcp Co according to Ref. 57. In separate field-dependent measurements, we determined the magnetic moments up to a magnetic field of $H = 50$ kOe for several temperatures, showing that the saturation values agree with the values of Ref. 57 within a statistical error of about 8%.

At $T = 10$ K, an external field with $H = 50$ kOe was applied perpendicular to the film plane in order to saturate the sample. Then the field was reduced to $H = 50$ Oe and the temperature was raised stepwise up to $T = 300$ K. At fixed temperatures, the magnetic moment m_H was measured from
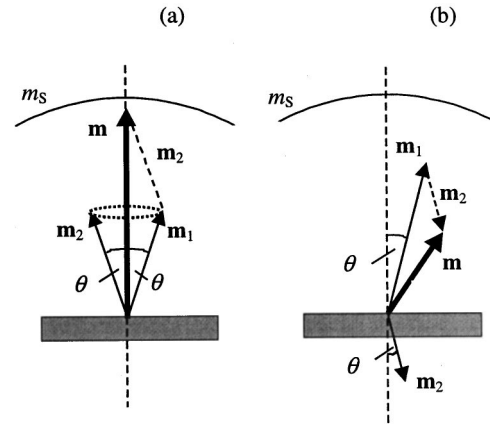

FIG. 5. Vector analysis of the effective magnetic moments $\mathbf{m}(T = 10\,\mathrm{K})$ measured for the Au(111)/16 Å Co/W sample with different magnetic history [see Figs. 4(a) and 4(b)].

$\theta_H = 0°$ to $\theta_H = 90°$. The vectors $\mathbf{m}(T)$ of the magnetic sample moment result from the maxima of $m_H(\theta_H, T)$ as a function of θ_H. After the saturation at $T = 10$ K, $m = |\mathbf{m}|$ is only slightly reduced with respect to the saturation moment m_S [Fig. 4(a)]. With increasing temperature, $\mathbf{m}$ rotates towards the film plane. At $T = 300$ K, $\mathbf{m}$ is nearly parallel to the film plane. The "lacking" amount $m_S - m$ has increased during the reorientation, but it is considerably smaller than m_S. Therefore, one can conclude that when the sample was saturated at $T = 10$ K a single-domain state was produced, and this remains stable with increasing temperature. At $T = 300$ K the sample was saturated parallel to the film plane with $H = 50$ kOe. At decreasing temperature, m_H was measured in the same manner ($H = 50$ Oe). Here $\mathbf{m}(T)$ first only shows small differences to the respective $\mathbf{m}(T)$ measured at increasing T. At $T \approx 180$ K one can recognize a bend in the curve of $|\mathbf{m}(T)|$. If T decreases further, m reduces more and more with respect to m_S. At $T = 10$ K the difference $m_S - m$ is even larger than m.

Similar behavior was observed for Au(111)/Co/W and Au(111)/Co/Au samples with other values of d_{Co}. Distinct states of domain splitting may be stabilized for the out-of-plane magnetization, as illustrated in Figs. 5(a) and 5(b), which correspond to the situation at $T = 10$ K of Figs. 4(a) and 4(b), respectively. The effective magnetic moment $\mathbf{m}$ is considered as composed of magnetic domains with moments $\mathbf{m}_i$ such that the conditions $\Sigma_i \mathbf{m}_i = \mathbf{m}$ and $\Sigma_i |\mathbf{m}_i| = m_S$ are fulfilled. We restrict ourselves to the discussion of two different $\mathbf{m}_i$. For reasons of symmetry, we can assume that the angles between $\mathbf{m}_1$ and $\mathbf{m}_2$ and the film normal are equal. In Fig. 5(b), m is considerably reduced with respect to m_S. In contrast to the situation of Fig. 5(a), the conditions $\Sigma_i \mathbf{m}_i = \mathbf{m}$ and $\Sigma_i |\mathbf{m}_i| = m_S$ may be simultaneously fulfilled only if the perpendicular components of $\mathbf{m}_i$ are different in sign. These considerations suggest that the evolution of the out-of-plane component at decreasing temperature is mainly affected by the formation of up and down magnetized domains, but the formation of in-plane magnetized domains during the transition cannot be ruled out. In order to investigate this in more detail, we used PNR (see also Sec. III A).
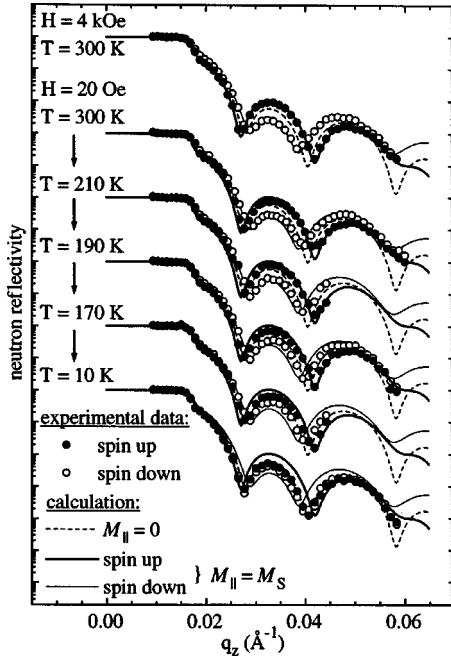
FIG. 6. Polarized neutron reflectivities of a Au(111)/16 Å Co/W sample measured for decreasing T.

Figure 6 shows some of the neutron reflectivity spectra measured in the temperature range from 300 K down to 10 K for the PNR sample Au(111)/Co/W with $d_{Co} = 16.0$ Å (Sec. III A). Before cooling, the external field, which was used to saturate the sample and to produce a defined remanent state, was turned off with exception of the guide field. Between 300 and 210 K no considerable changes of the spectra were observable. The splitting between spin-up and spin-down reflectivities was only slightly reduced from the saturated state. From 210 to 150 K the splitting decreased continuously. Below 150 K only a small splitting remained. In order to quantify the behavior of the in-plane component of the magnetization, the spin asymmetry S,

$$S = \frac{R^+ - R^-}{R^+ + R^-}, \quad (3)$$

with the reflectivities R^+ and R^- of spin-up and spin-down neutrons was considered. The simulated $S(q_z)$ scales approximately linearly with the in-plane component $M_\parallel$ of the magnetization, which gives the possibility to determine the absolute value of $M_\parallel$ directly by comparing simulated and the measured $S(q_z)$. Figure 7 shows the evaluated $M_\parallel$ normalized to the values of M_S of Ref. 57 as a function of T. The diagram also contains the results measured for an Al$_2$O$_3$(11$\bar{2}$0)/W(110)/Au(111)/Co/Au sample with $d_{Co} = 19$ Å at the neutron reflectometer ADAM (ILL, Grenoble).[61] In this case we also measured the magnetic moments for increasing T immediately after reaching $T = 10$ K *without changing* the magnetic field. Within the error bars the values of $M_\parallel/M_S$ were the same as for decreasing T. Thus the change of $M_\parallel$ is reversible.

The spin-dependent neutron reflectivities contain information about domain formation, too. In the case of a decay into
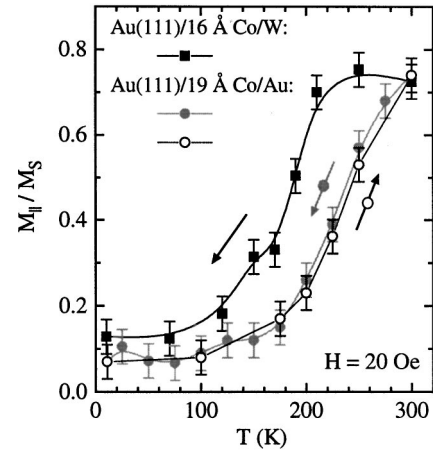

FIG. 7. Normalized in-plane magnetization component $M_\parallel/M_s$ of a Au(111)/16 Å Co/W and a Au(111)/19 Å Co/Au sample vs temperature T.

in-plane magnetized domains with a mean lateral diameter D, which is larger than the lateral or longitudinal coherence length l_c^{long} of the neutrons,[48] one can take for granted that the reflected *intensities* of the different domains add up to the total reflected intensity. With the experimental parameters $\Delta q \approx 0.002$ Å^{-1} and with $\lambda = 4.66$ Å (V6), we can estimate $l_c^{long} \approx 28 \, \mu$m at $q_z = 0.03$ Å^{-1} (for $q_z = 0.04$ and 0.05 Å^{-1}, we find $l_c^{long} \approx 21$ and 17 μm, respectively). We now assume that the in-plane magnetization decays into large domains, which are magnetized parallel and antiparallel with respect to the virtual saturated state parallel to the polarization axis of the neutrons and which occupy the parts $1-\gamma$ and γ of the lateral sample area. The magnetization within a domain is assumed to be homogeneous and equal to the saturation magnetization M_S. The total in-plane component of the magnetization is then given by $M_\parallel = (1-\gamma)M_s + \gamma(-M_s) = (1-2\gamma)M_s$. Within this domain model the observable total neutron reflectivity is an incoherent, weighted sum of the reflectivities corresponding to the respective domains. One has to take into account that spin-up (spin-down) neutrons reflected from an antiparallel magnetized domain are reflected as spin-down (spin-up) neutrons for the case of saturation. The experimental data shown in Fig. 8 are the same as in Fig. 6. The calculations (solid lines) for the model of a reduced but *homogeneous* in-plane magnetization and the domain model described above were fitted to the experimental reflectivities in the following manner: first, we calculated the spin asymmetries $S(q_z)$ for both models as a function of $M_\parallel$. These were compared with the measured spin asymmetries around the Bragg peak position at $q_z = 0.033$ Å^{-1}. The comparison gives the experimental values of $M_\parallel$ with which we finally calculated the reflectivity profiles. As one can see, there is an obvious discrepancy in the minima of reflectivity between the domain model and experimental values [Fig. 8(b)]. In contrast to this, the reflectivities, which were calculated for the homogeneous magnetized state, are in much better agreement with the experimental data [Fig. 8(a)]. This shows that decay into large in-plane magnetized domains does not occur. What about the formation of very small do-
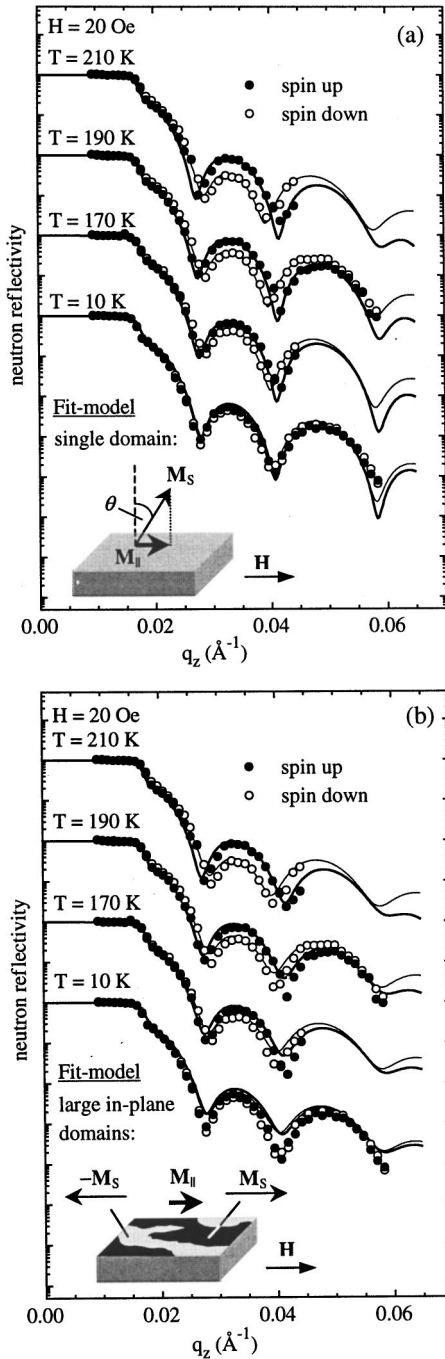
FIG. 8. Comparison of measured with calculated neutron reflectivities for the Au(111)/16 Å Co/W sample. The underlaying magnetization models (see text) are represented schematically.

mains? In order to deal with this aspect, we also investigated the off-specular ($q_x \neq 0$) neutron intensity by measuring rocking scans at the Bragg peak ($q_z = 0.033$ Å^{-1}) for different temperatures. According to the diffraction relation $\Delta q_x \cong 2\pi/D$, one would expect a broadening of the peaks if the magnetization decays into domains with a mean lateral diameter D which is much smaller than the longitudinal coherence length l_c^{long}. We did not observe a significant change of their width in our experiments. However, up to now off-specular neutron intensity of magnetic origin has only been

observed for periodic, antiferromagnetically coupled multilayers.[62–64] The investigation of single ultrathin magnetic layers is complicated by the fact that the amount of magnetic material is much smaller than in multilayers and that the maxima of reflectivity due to nuclear and magnetic scattering are at fairly the same position so that a possible magnetic off-specular intensity may be obscured by the total reflected intensity. Further experiments with the new position-sensitive detectors (PSD's), which allow measurements with a higher resolution and sensitivity, may help to clarify the question as to whether off-specular neutron intensity due to magnetic roughness is also observable for single ultrathin magnetic films.

In both samples Au(111)/16 Å Co/W and Au(111)/19 Å Co/Au, the in-plane component of the magnetization at low fields was found to decrease continuously with decreasing T (Fig. 7). If the difference $\Delta d_{Co}^* = 14.5$ Å $- 12.8$ Å $= 1.7$ Å between the reorientation thicknesses d_{Co}^* of both systems at $T = 300$ K (Table I) was independent of temperature, one would expect that the in-plane magnetization of the Au(111)/Co/Au sample decreases at lower temperature in comparison to the Au(111)/Co/W sample, since its Co film is thicker by 3 Å. Obviously, the opposite situation is the case. The thickness region of perpendicular anisotropy seems to increase more with decreasing temperature in case of an Au overlayer. That will be investigated in more detail in the following section.

C. Magnetic phase diagrams

The experimental proof of the conclusion drawn at the end of Sec. III B requires a systematic measurement of the in- and out-of-plane magnetization in both systems as a function of Co film thickness and temperature. For that purpose a Au(111)/Co/W and a Au(111)/Co/Au sample series each with samples of different Co film thickness were investigated by means of SQUID magnetometry, as was described in Sec. III B. We restricted ourselves to measurements with $\theta_H = 0°$ and $\theta_H = 90°$. In order to describe the results in a compact manner, we introduce the quantity

$$P = \frac{M_{\perp,T\uparrow} - m_{\parallel,T\downarrow}}{m_{\perp,T\uparrow} + m_{\parallel,T\downarrow}}, \quad P = P(d_{Co}, T), \quad (4)$$

which compares the in- and out-of-plane components $m_{\parallel,T\downarrow}$ and $m_{\perp,T\uparrow}$ of the sample moment measured for decreasing and increasing temperature, respectively. Due to the small applied field ($H = 50$ Oe), $m_{\perp,T\uparrow}$ and $m_{\parallel,T\downarrow}$ have always the same sign, and therefore P can have values only between -1 and $+1$. Here P is positive in the case of a perpendicular anisotropy and negative if the easy axis of magnetization is in the film plane. $P(d_{Co}, T)$ is represented as a gray scale map for each of both systems in Fig. 9. Data points were measured in distances of $\Delta d_{Co} = 1.3$ Å starting at $d_{Co} = 7.6$ Å up to $d_{Co} = 23.2$ Å for the system Au(111)/Co/W [Fig. 9(a)] and in distances of $\Delta d_{Co} = 3.0$ Å starting at $d_{Co} = 9.0$ Å up to $d_{Co} = 33.0$ Å for the system Au(111)/Co/Au [Fig. 9(b)]. The temperature was varied between 10 and 300 K in steps of $\Delta T = 10$ K. Both diagrams show that the thick-
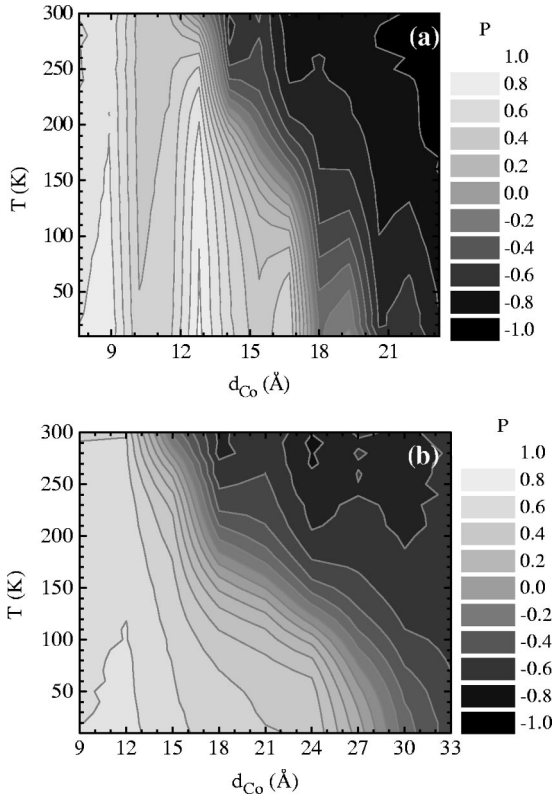
FIG. 9. Magnetic phase diagrams of (a) Au(111)/Co/W and (b) Au(111)/Co/Au. The value $P = +1$ ($P = -1$) corresponds to a magnetization perpendicular (parallel) to the film plane. Please note that the thickness scales of both diagrams are different.
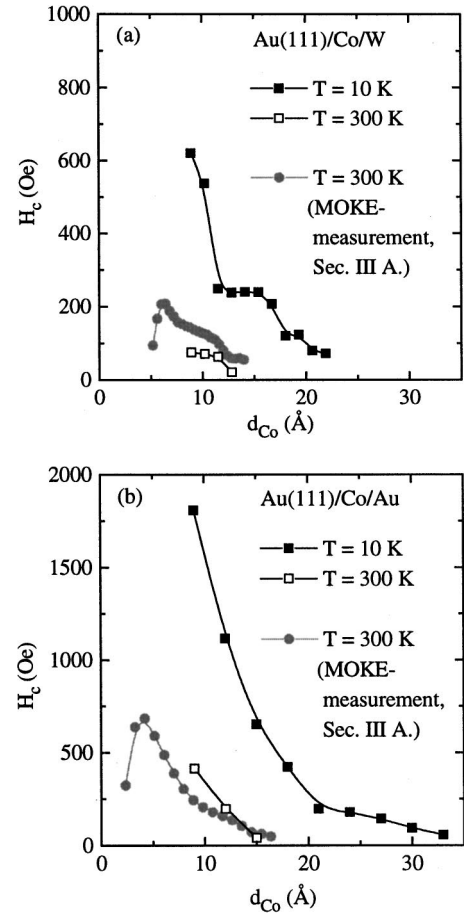

FIG. 10. Coercive fields of Au(111)/Co/W and Au(111)/Co/Au at $T = 10$ and 300 K for magnetic fields applied perpendicular to the film plane vs Co film thicknesses d_{Co}.

ness region of perpendicular anisotropy increases with decreasing temperature. The increase is significantly stronger for Au(111)/Co/Au (as supposed at the end of Sec. III B). The difference between $d_{Co,P=0}$ of both systems is less than 2 Å at $T = 300$ K, but about 10 Å at $T = 10$ K. Further, one can recognize that the transitions develop over a wider range of film thickness for this system Au(111)/Co/Au. While the reorientation thickness is mainly determined by the interface anisotropy constant of first order, K_1^S (see Sec. I), the second order K_2^S determines the width of the transition.[7] Comparison between the phase diagrams suggests that the surface anisotropy constants for Au(111)/Co/Au are larger and also more T dependent than those of Au(111)/Co/W.

We also performed field-dependent measurements at $T = 10$ and 300 K for magnetic fields $-50 \text{ kOe} \leqslant H \leqslant 50 \text{ kOe}$ applied both parallel and perpendicular to the film plane. The magnetization curves confirmed the differences between the reorientation thicknesses of both systems found in the temperature-dependent measurements at low constant field, but they provide some further information. In Figs. 10(a) and 10(b), the perpendicular ($\theta_H = 0°$) coercive fields H_c are shown as a function of d_{Co}. Since only a few of the prepared samples revealed a perpendicular anisotropy at $T = 300$ K, we show for comparison the coercive fields measured with MOKE on the respective Co wedges (Sec. III A). As expected, the coercive fields are larger at low temperature and significantly larger for the system Au(111)/Co/Au. Moreover,

the curves $H_c(d_{Co})$ exhibit striking features for each system, i.e., a shoulder for Au(111)/Co/W and a bend for Au(111)/Co/Au. These features are more pronounced at 10 K and, as for the SRT, shifted to higher values of Co film thickness.

What are the reasons for the difference in the thickness and temperature dependence behavior of the two systems? One possible explanation is the presence of epitaxial strain at the interfaces, which depends in a different way on d_{Co} and T. The LEED spots of the 30-Å-thick W and Au overlayers were only weak and diffuse in our study. On the other hand, we found well-pronounced LEED spots for the additional 200-Å-thick Au overlayers, which were prepared for the PNR samples (Sec. II). This shows that further epitaxial growth onto the Co film and overlayers occurs. However, a systematic growth study including strain analysis was only performed for the Co layer as a function of d_{Co} (Sec. II), but not yet for the overlayers, which would require measurements as a function of d_{Co} *and* overlayer thickness. Another possibility for the observed differences could be the sensitivity of the surface or interface anisotropy to the detailed electronic structure. To get more information about this contribution, calculations performed for the temperature-dependent electronic band structure of both Co/overlayer interfaces or corresponding experimental studies would be fruitful.

IV. CONCLUSIONS

In summary, we have studied the spin-reorientation transition of Au(111)/Co films prepared on $Al_2O_3(11\bar{2}0)$ single crystals as a function of Co film thickness and temperature. We used magneto-optical Kerr-effect (MOKE) measurements, polarized neutron reflectometry (PNR), and SQUID magnetometry as complementary methods.

The *thickness-driven SRT* was studied at $T = 300$ K prior and after coverage with W and Au overlayers. Both overlayers shift the SRT to larger values of the Co film thickness, which is, for W, 1.7 Å smaller than in the case of Au. Studying the *temperature-driven SRT* of Au(111)/Co/W and Au(111)/Co/Au samples, we observed a strong dependence of the magnetization on the magnetic history at low temperatures, which is attributed to a different degree of domain splitting of the perpendicular magnetization component. The *magnetic phase diagrams* of both systems showed that the reorientation thickness of the Co layer in Au(111)/Co/Au is less than 2 Å larger than in Au(111)/Co/W at $T = 300$ K, but the difference increases with decreasing temperature and amounts to about 10 Å at $T = 10$ K. Striking features were found for both systems in the curves of perpendicular coercive fields as a function of Co film thickness.

In no hysteresis and low-field measurements have we observed a situation in which both the in-plane and out-of-plane components of the magnetization vanish simultaneously. This finding is in agreement with other studies of Au(111)/Co (Refs. 2 and 23) and further Co-based systems, e.g., Ru(0001)/Co.[18] In contrast to this, *simultaneously* vanishing or at least strongly reduced out-of-plane *and* in-plane magnetization components were observed in the region of transition for the systems Ag(100)/Fe (Refs. 14 and 16) and Cu(100)/Fe (Refs. 14 and 15). While it was first speculated that an intermediate paramagnetic state exists, it seems more probable that this phenomenology is due to pronounced domain formations.[15] Therefore, both systems might be interesting for a study of the specular and off-specular neutron reflectivity. Without overlayers these experiments require UHV conditions, but as shown recently,[45] *in situ* PNR measurements can be performed.

*Author to whom correspondence should be addressed. FAX: +49-30-8062-2523. Electronic address: maletta@hmi.de

[1] L. Néel, J. Phys. Radium **15**, 225 (1954).

[2] C. Chappert and P. Bruno, J. Appl. Phys. **64**, 5736 (1988).

[3] P. Bruno, in *Magnetismus von Festkörpern und Grenzflächen*, edited by P. H. Dederichs, P. Grünberg, and W. Zinn (KFA Jülich, Jülich, 1993).

[4] H. J. G. Draaisma and W. J. M. de Jonge, J. Appl. Phys. **64**, 3610 (1988).

[5] W. J. M. de Jonge, P. J. H. Bloemen, and F. J. A. den Broeder, in *Ultrathin Magnetic Structures*, edited by J. A. C. Bland and B. Heinrich (Springer-Verlag, Berlin, 1994), Vol. 1.

[6] H. Fritzsche, J. Kohlhepp, H. J. Elmers, and U. Gradmann, Phys. Rev. B **49**, 15 665 (1994).

[7] Y. Millev and J. Kirschner, Phys. Rev. B **54**, 4137 (1996).

[8] P. J. Jensen and K. H. Bennemann, Solid State Commun. **100**, 585 (1996).

[9] P. J. Jensen and K. H. Bennemann, Solid State Commun. **105**, 577 (1998).

[10] A. Hucht and K. D. Usadel, J. Magn. Magn. Mater. **203**, 88 (1999).

[11] S. T. Chui, Phys. Rev. B **50**, 12 559 (1994).

[12] A. Hucht, A. Moschel, and K. D. Usadel, J. Magn. Magn. Mater. **148**, 32 (1995).

[13] T. Herrmann, M. Potthoff, and W. Nolting, Phys. Rev. B **58**, 831 (1998).

[14] D. P. Pappas, C. R. Brundle, and H. Hopster, Phys. Rev. B **45**, 8169 (1992).

[15] R. Allenspach, J. Magn. Magn. Mater. **129**, 160 (1994).

[16] Z. Q. Qiu, J. Pearson, and S. D. Bader, Phys. Rev. Lett. **70**, 1006 (1993).

[17] H. Fritzsche, J. Kohlhepp, H. J. Elmers, and U. Gradmann, in *Common Themes and Mechanisms of Epitaxial Growth*, edited by P. Fuoss, J. Tasao, D.W. Kisker, A. Zangwill, and T. F. Kuech, MRS Symposia Proceedings No. 312 (Materials Research Society, Pittsburgh, 1993), p. 321.

[18] G. Garreau, E. Beaurepaire, K. Ounadjela, and M. Farle, Phys. Rev. B **53**, 1083 (1996).

[19] T. Nawrath, B. Damaske, O. Schulte, and W. Felsch, Phys. Rev. B **55**, 3071 (1997).

[20] J. Kohlhepp and U. Gradmann, J. Magn. Magn. Mater. **139**, 347 (1995).

[21] C. Chappert, K. Le Dang, P. Beauvillain, H. Hurdequint, and D. Renard, Phys. Rev. B **34**, 3192 (1996).

[22] R. Allenspach, M. Stampanoni, and A. Bischof, Phys. Rev. Lett. **65**, 3344 (1990).

[23] V. Grolier, J. Ferré, A. Maziewski, E. Stefanowicz, and D. Renard, J. Appl. Phys. **73**, 5939 (1993).

[24] J. Ferré, J. P. Jamet, J. Pommier, P. Beauvillain, C. Chappert, R. Mégy, and P. Veillet, J. Magn. Magn. Mater. **174**, 77 (1997).

[25] M. Dreyer, M. Kleiber, A. Wadas, and R. Wiesendanger, Phys. Rev. B **59**, 4273 (1999).

[26] M. Farle, B. Mirwald-Schulz, A. N. Anisimov, W. Platow, and K. Baberschke, Phys. Rev. B **55**, 3708 (1997).

[27] M. Farle, Rep. Prog. Phys. **61**, 755 (1998).

[28] H.-J. Elmers and U. Gradmann, Appl. Phys. A: Solids Surf. **51**, 255 (1990).

[29] Y. Li, C. Polaczyk, and D. Riegel, Thin Solid Films **317**, 310 (1998).

[30] G. Lugert, G. Bayreuther, S. Lehner, G. Gruber, and P. Bruno, in *Magnetic Materials: Microstructure and Properties*, edited by T. Suzuki, Y. Sugita, B. M. Clemens, K. Ouchi, and D. E. Laughlin, MRS Symposia Proceedings No. 232 (Materials Research Society, Pittsburgh, 1991), p. 97.

[31] N. D. Mermin and H. Wagner, Phys. Rev. Lett. **17**, 1133 (1966).

[32] D. Pescia and V. L. Pokrovsky, Phys. Rev. Lett. **65**, 2599 (1990).

[33] R. P. Erickson and D. L. Mills, Phys. Rev. B **46**, 861 (1992).

[34] D. K. Morr, P. J. Jensen, and K. H. Bennemann, Surf. Sci. **307–309**, 1109 (1994).

[35] M. Bander and D. L. Mills, Phys. Rev. B **38**, 12 015 (1988).

[36] Y. Yafet and E. M. Gyorgy, Phys. Rev. B **38**, 9145 (1988).

[37] R. Czech and J. Villain, J. Phys.: Condens. Matter **1**, 619 (1989).

[38] B. Kaplan and G. A. Gehring, J. Magn. Magn. Mater. **128**, 111 (1993).

[39] P. J. Jensen and K. H. Bennemann, Phys. Rev. B **52**, 16 012 (1995).

[40] I. Booth, A. B. MacIsaac, J. P. Whitehead, and K. De'Bell, Phys. Rev. Lett. **75**, 950 (1995).

[41] A. B. MacIsaac, K. De'Bell, and J. P. Whitehead, Phys. Rev. Lett. **80**, 616 (1998).

[42] H. Fritzsche, J. Kohlhepp, and U. Gradmann, Phys. Rev. B **51**, 15 933 (1995).

[43] H. Fritzsche, J. Kohlhepp, and U. Gradmann, J. Magn. Magn. Mater. **148**, 154 (1995).

[44] R. Sellmann, H. Fritzsche, H. Maletta, V. Leiner, and R. Siebrecht, Phys. Rev. B **63**, 224415 (2001).

[45] T. Nawrath, H. Fritzsche, F. Klose, J. Nowikow, and H. Maletta, Phys. Rev. B **60**, 9525 (1999).

[46] J. P. Renard, in *Magnetic Properties of Matter*, edited by G. Asti, D. Fiorani, and F. Lucari (World Scientific Singapore, 1991).

[47] C. Chappert, P. Beauvillain, P. Bruno, J. P. Chauyineau, M. Galtier, K. Le Dang, C. Marlière, R. Mégy, D. Renard, J. P. Renard, J. Seiden, F. Trigui, P. Veillet, and E. Vélu, J. Magn. Magn. Mater. **93**, 319 (1991).

[48] J. A. C. Bland, in *Ultrathin Magnetic Structures*, edited by J. A. C. Bland and B. Heinrich (Springer-Verlag, Berlin, 1994), Vol. 1.

[49] J. Zak, R. Moog, C. Liu, and S. D. Bader, J. Magn. Magn. Mater. **89**, 107 (1990).

[50] G. P. Felcher, Phys. Rev. B **24**, 1595 (1981).

[51] J. A. C. Bland, D. Pescia, R. F. Willis, and O. Schaerpf, Phys. Scr. **35**, 528 (1987).

[52] H. Zabel, Physica B **198**, 165 (1994).

[53] J. F. Ankner and G. P. Felcher, J. Magn. Magn. Mater. **200**, 741 (1999).

[54] F. Mezei, R. Golub, F. Klose, and H. Toews, Physica B **213-214**, 898 (1995).

[55] Model calculations were carried out with the software REFLECTIVITY TOOL PARRATT 32 (HMI, Berlin, 1999).

[56] L. G. Parratt, Phys. Rev. **95**, 359 (1954).

[57] M. B. Stearns, in *Magnetic Properties of Metals*, Landolt-Börnstein, New Series, Group III, Vol. 19a, edited by H. P. J. Wijn (Springer-Verlag, Berlin, 1986).

[58] V. F. Sears, Neutron News **3**, 26 (1992).

[59] G. L. Squires, *Introduction to the Theory of Thermal Neutron Scattering* (Dover, Mineola, NY, 1996).

[60] S. J. Blundell and J. A. C. Bland, Phys. Rev. B **46**, 3391 (1992).

[61] A. Schreyer, R. Siebrecht, U. Englisch, U. Pietsch, and H. Zabel, Physica B **248**, 349 (1998).

[62] G. P. Felcher, Physica B **198**, 150 (1994).

[63] Ch. Rehm, D. Nagengast, F. Klose, H. Maletta, and A. Weidinger, Europhys. Lett. **38**, 61 (1997).

[64] J. A. Borchers, J. A. Dura, J. Unguris, D. Tulchinski, M. H. Kelley, and C. F. Majkrzak, Phys. Rev. Lett. **82**, 2796 (1999).